Proton Cross-Sections from Heavy-Ion Data in GaAs Devices

D.L. Hansen

Abstract—**This paper reports on the calculation of proton SEU cross section from heavy-ion data in GaAs devices. A number of different models are used, however in each, accommodations must be made to account for the fact that the density and ionization energy of GaAs differs from that of Si. Model accuracy is checked using data on proton and heavy-ion cross sections from the published literature.**

Index Terms—**SEU, single event upset, proton induced SEU, SEU in deep submicron devices, prediction tool, heavy ion**

I. Introduction

There are a number of useful models for calculating the cross section of proton SEE from heavy-ion data [1]-[7]. In general these SEE calculations are predicated on the use of proton – Si interaction models to determine the secondary products and the use of the heavy-ion data to determine the effect of the secondaries. Less work has been done to perform these types of calculations on III-V devices, primarily because III-V devices do not enjoy the widespread use in space that Si devices do. However, while there may not be widespread demand to perform these calculations, applying the models to III-V devices provides additional validation of the models used.

This paper evaluates a number of models to determine their ability to calculate high-energy proton SEE cross sections of GaAs devices from heavy-ion data. The focus of this paper is restricted to models generally available to the radiation community, and the models are evaluated using data provided in the open literature [8]-[13] as test cases.

II. Modeling and Data Collection

In order to develop a suitable data set for analysis, a number of papers in the open literature that include both proton and heavy-ion data were surveyed (Table I). The proton and heavy-ion data was digitized and placed into a data base to facilitate automatic processing. For comparison purposes, an InP device [13] was included with the other devices modeled. We note that the base and collector are made from InGaAs in a InP transistor [14]-[16] with the InP being concentrated in the subcollector layer. Thus the Ga and As atoms are concentrated at the junctions.

It should be noted that one possible source of error in these calculations arises for the units on the LET. In most cyclotrons, the LET given is for Si semiconductors. In several of the papers, LET units corresponding to LET for the test data was not explicitly described as LET in Si or GaAs. All LET values from the literature were assumed to be LET in GaAs, and the LET in Si values given by the "Submit a CREME-MC run" page were converted to LET in GaAs.

TABLE I
Feature size, Technology and Device Type of Data Analyzed

Reference	Technology	Device Description
Cutchin [8]	GaAs C-HIGFET	1k x 1 SRAM
Garcia [12]	GaAs MESFET	Power MESFET
Marshall [9]	GaAs HIGFET	SCFL Shift Register
Weatherford [10]	GaAs MESFET	1k SRAM
Weatherford [11]	GaAs C-EJFET	256b SRAM
Hansen [13]	InP HBT	Shift Register

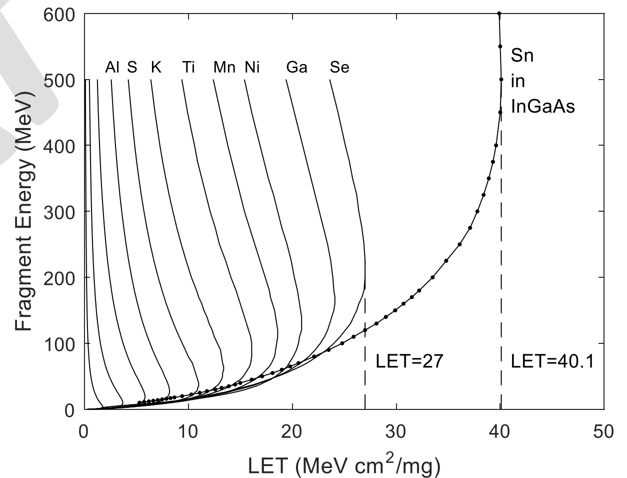

Fig. 1 LET and fragment energy in GaAs. Curve for Sn in InGaAs was included to show the maximum LET for the InP device in [13]. Curves were calculated using SRIM [18].

Three models from the literature with closed form equations were chosen. They were used to compare proton and heavy-ion cross-section data pulled from the literature. However in each case modifications were made to the model to account for the fact that we are modeling GaAs and not Si devices. In the PROFIT model [1] the proton cross section (σ_p) is calculated based on the heavy ion cross section (σ_{HI}), the assumed charge collection depth (d), the density in numbers of atoms per cm^3 and the nuclear cross section for proton interactions (σ_{nuc})

Manuscript received October 9, 2001. .
D. L. Hansen is with Data Devices Corp., San Diego, CA 92123 USA.
e-mail:hansen@ddc-web.com.

DRAFT

$$\sigma_p = nd(\sigma_{HI})(\sigma_{nuc}). \quad (1)$$

For the GaAs devices we use a density of 4.4E22 atoms / cm^3, and a charge collection depth of 3 µm. Following the results of [17] we scale the Si nuclear cross section (σ_{nuc}[Si]) by 1.7 to get the GaAs nuclear cross section

$$\sigma_{nuc}[\text{GaAs}] = \sigma_{nuc}[\text{Si}] \,/\, 1.7. \quad (2)$$

We also assume, and that all secondary products from the proton-GaAs interaction have the maximum LET (27 MeV cm^2/mg). This is based on calculations from SRIM [18] (Fig. 1) that indicate the maximum LET from a Ga – proton interaction would be 27 MeV cm^2/mg. For the InP device [13] we use the LET curve for Sn fragment in InGaAs (Fig. 1) and note the maximum LET produced following proton irradiation is 40.1 MeV cm^2/mg. Using the maximum LET for the secondaries is a conservative assumption that should provide an upper bound to the proton cross section. Results are summarized in Fig. 2-3

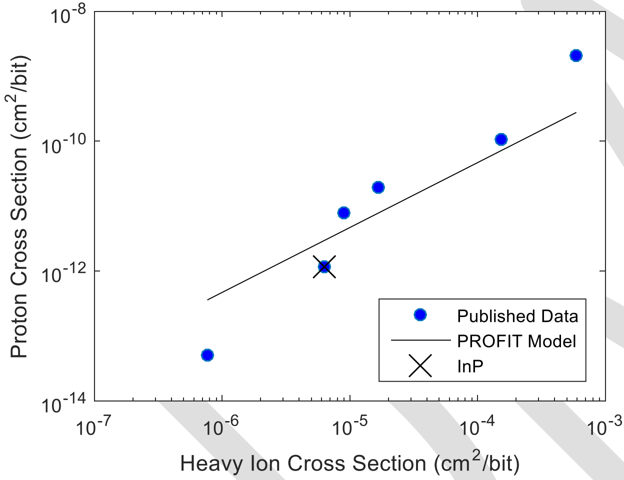

Fig. 2 Proton cross-section as a function of heavy-ion cross section at LET=27 MeV cm^2/mg for the PROFIT model [1] and published data.

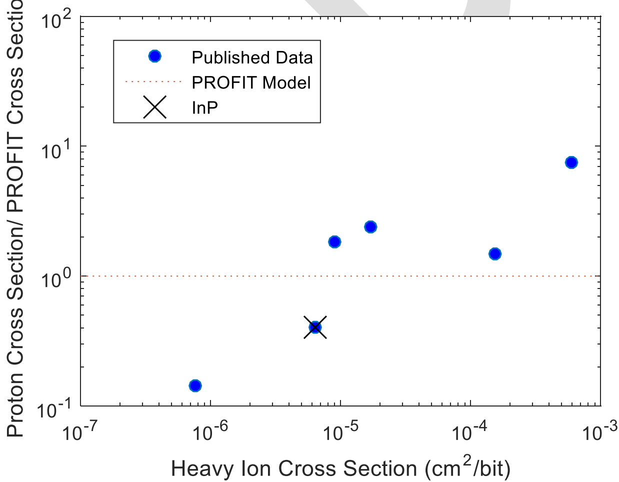

Fig. 3 Ratio of proton data to the predicted proton cross section for the PROFIT model [1] and published data.

The model proposed by Edmonds [2] is derived from an integral over LET (L), given by

$$\sigma_p(E) = \beta(E) \times a^{-1} \int \sigma_{HI} L^{-2}\, dL. \quad (3)$$

Here a is a unit conversion between LET and liberated charge. Here we use a=1.77E-10 C/cm (MeV cm^2/mg) $^{-1}$ for GaAs instead of the value given for Si in [2]. The β(E) value is the burst generation rate from Normand [19] divided by 1.7 to have a value appropriate for GaAs [17]. In this case the cross section calculation requires an integral over the full cross section curve. For the modeling performed here (Fig. 4 - 5), we used a Weibull fit of the data with a threshold and saturated cross section chosen to ensure the Weibull provides an upper bound to the data.

The model proposed by Barak et al [3] is derived from the ratio of the figure of merit (FOM) equations presented by Petersen [20]. This model calculates the ratio of the proton and heavy-ion saturated cross sections using the LET at 25% of the saturated cross section (L_{25})

$$\sigma_{p\infty} = (\sigma_{HI\infty}/1.7)\ 2.22\cdot 10^{-5}\ (L_{25})^{-2} \quad (4)$$

where the ∞ subscript indicates the saturated cross section. The Petersen FOM equations were derived empirically based on data from Si parts (Fig. 6 - 7). Again, the factor of 1.7 is used to convert the model to apply to GaAs instead of Si.

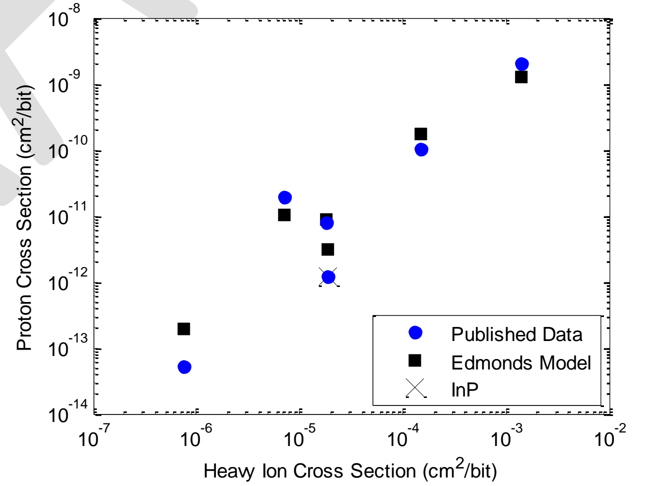

Fig. 4 Proton cross-section as a function of heavy-ion cross section at saturation ($\sigma_{HI\infty}$). For the Edmonds model Eq. 3 [2] and published data.

TABLE II
RATIO OF PROTON CROSS SECTION TO MODEL FOR DATA ANALYZED

Reference	PROFIT [1]	Edmonds [2]	Barak [3]	CREME-MC
Cutchin [8]	0.14	0.26	0.11	0.13
Garcia [12]	7.46	1.6	0.34	1.7
Marshall [9]	1.47	0.60	0.35	0.45
Hansen [13]	0.48	0.91	0.51	0.14
Weatherford [11]	1.85	0.39	1.2	0.48
Weatherford [10]	2.41	1.81	2.5	0.73
Average	2.30	0.93	0.84	0.61

DRAFT

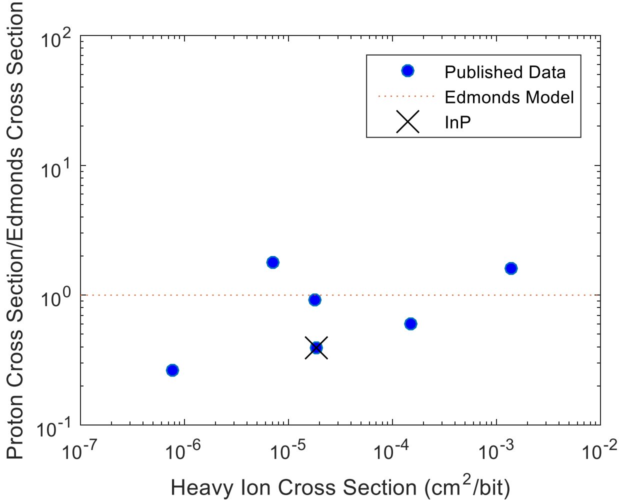

Fig. 5 Ratio of proton data to the predicted proton cross section for the Edmonds model [2] and published data

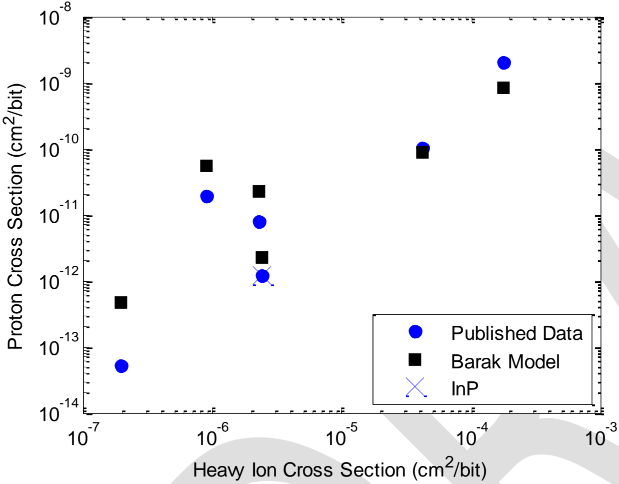

Fig. 6 Proton-cross section as a function of heavy-ion cross section at saturation ($\sigma_{HI\infty}$). The Barak model [3] is shown with the published data.

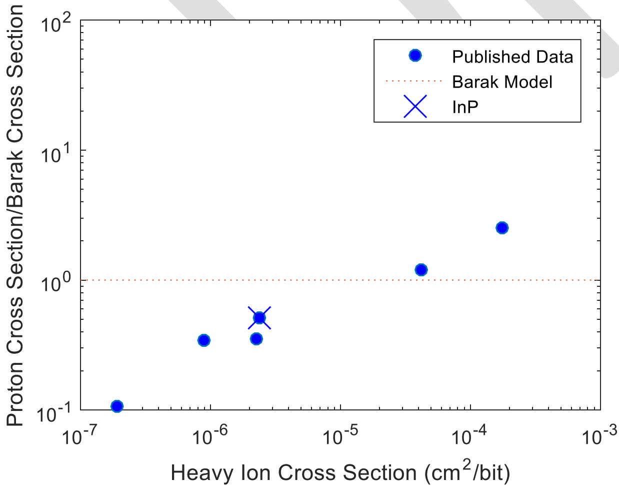

Fig. 7 Ratio of proton data to the predicted proton cross section for the Barak model [3] is shown with the published data.

In general, all three models describe the data well, in the two cases where the models do most poorly, the heavy ion cross section curves covered less than an order of magnitude between the lowest and highest cross section points. [10], [12]. Thus the difference between the models and underscores the importance of collecting data that provides a good characterization of the threshold [21].

All three models are able to predict the proton cross-sections within an order of magnitude for the devices studied here, including the InP device. Of these, the model in [2] was the most accurate (Table II). The models consistently underestimate the measured cross section for the device from [10] this is likely a result of the fact that the data in [10] was not collected at a LET greater than 6.5 MeV cm^2/mg, and so the saturated cross section may not be fully captured.

The greatest disagreement between the model and the data is for the device described in [12]. In this case the cross sections given in the paper are for SEB and thus the saturated cross-section may not represent the lateral dimensions of a single RPP, but instead may be the cumulative cross-section for multiple sensitive volumes.

III. Modeling with CREME-MC

The CREME-MC suite of tools allows the user to perform Monte-Carlo simulations of a variety of incident particles upon a sensitive volume modeled by a single or a group of RPPs. It is widely available to the radiation community on the web [22]. CREME-MC allows the user to input a number of different parameters based on the physical operation of the device. These would include multiple sensitive volumes with adjustable charge-collection efficiencies and size [23] - [25] a variable "stack" to allow for different materials in the layers of the device [7]; as well as the critical charge for the device.

TABLE III Ions Used in CREME-MC Simulations

Ion	Energy (MeV)	LET(GaAs) (MeV cm^2/mg)
C	210	1.1
N	210	1.7
Ne	500	2.3
Ne	300	3.4
Ar	1000	7.4
Ar	600	10.7
Kr	1260	38.4

The modeling performed here uses a simplified approach in that all parameters are derived from the SEE data without the benefit of TCAD modeling. The sensitive volume is a single RPP box. While this may be less physically correct than the multiple sensitive volumes which can be used in CREME-MC modeling, it has the advantage of simplicity, speed of calculation, and the fact that it has been successfully applied in many cases to determine device response [26]. Additionally, the stack used is a single box 1000 µm × 1000 µm and 500 µm deep, comprised entirely of GaAs. This simplification is not unreasonable since it has been previously shown that in low threshold devices; the upset contribution from heavy metals is small relative to the bulk contribution [27].

A. *Selection of Parameter Definitions*

For all devices, the RPP lateral dimensions were chosen as the square root of the saturated cross section, and the charge collection depth (d) was set as 3µm. The depth was chosen as

DRAFT

a reasonable compromise based on charge collection modeling data from all devices provided in the papers referenced. LET threshold (L_{th}) and saturated cross section ($\sigma_{HI\infty}$) were based on the minimum LET used in testing and the maximum heavy-ion cross section. The initial estimate for critical charge in the simulations is derived from the heavy ion data using the expression:

$$E_{crit} = \rho \times L_{th} \times d \quad (4)$$

where ρ is the density of GaAs. In these simulations, the expression $(\sigma_{HI\infty})^{1/2}$ provides the initial estimate of both the lateral dimensions of the sensitive volume. The heavy-ion data was then simulated in CREME-MC using some or all of the ions in Table III. The simulations were run in detailed mode with enough particles selected to reach the 1 hr. time limit for calculations. This generated the curves shown in Fig. 8 - 13. The best value for the critical energy from the CREME-MC plots in is determined as the energy that minimizes the quantity:

$$\sum_{i} log([\sigma_{sim}(i) - \sigma_{data}(i)]^2) \quad (5)$$

where $\sigma_{data}(i)$ and $\sigma_{sim}(i)$ represent the cross section for the data and simulation (respectively) at a specific energy for each of the LETs shown in Table III. Here the *log* in the sum emphasizes the threshold region in the fit. These are summarized in Table IV, along with the E_{crit} values given in the papers from which the data was taken. Deviations between the values calculated here and the values in the literature are a natural result of different assumptions regarding the sensitive volume.

TABLE IV CALCULATED E_{CRIT}

Reference	CREME-MC Heavy Ion E_{crit} (MeV)	Eq. 4 E_{crit} (MeV)	E_{crit} From Paper (MeV)
Cutchin [8]	3.09	3.0	1.5
Garcia [12]	2.14	3.1	27.9
Marshall [9]	2.14	4.8	1.5
Hansen [13]	2.14	4.2	--
Weatherford [10]	0.98	0.8	1.5 – 5.1
Weatherford [11]	1.12	1.2	0.9

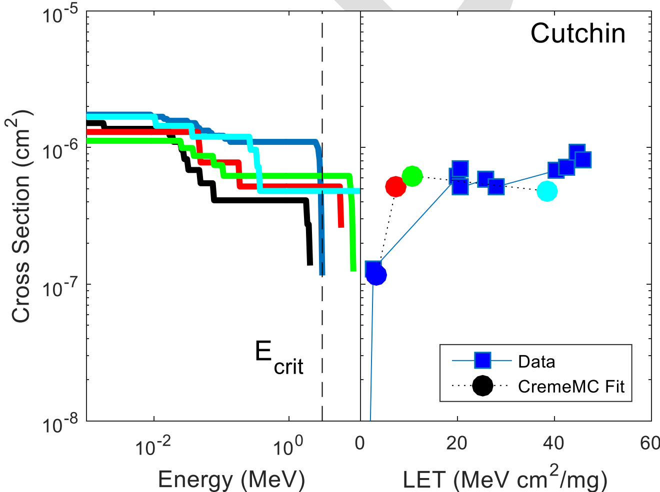

Fig. 8 Cross section curves generated by CREME-MC (left) and CREME-MC model compared to published data for [8]. Vertical dashed line indicates E_{crit} used to obtain the fit to the heavy ion data.

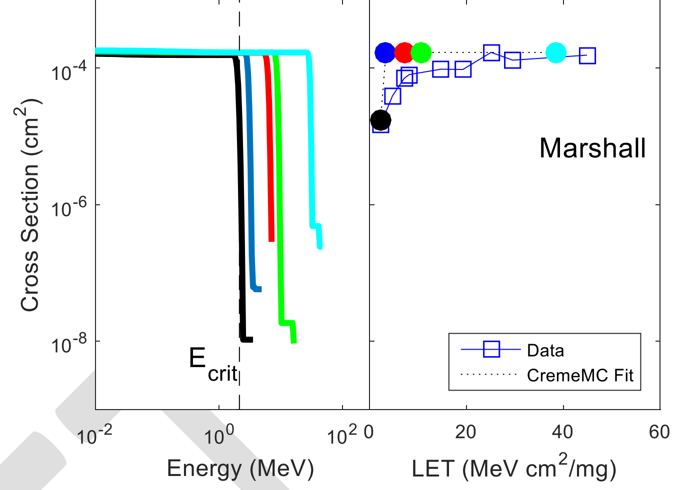

Fig. 9 Cross section curves generated by CREME-MC (left) and CREME-MC model compared to published data for [9]. Vertical dashed line indicates E_{crit} used to obtain the fit to the heavy ion data.

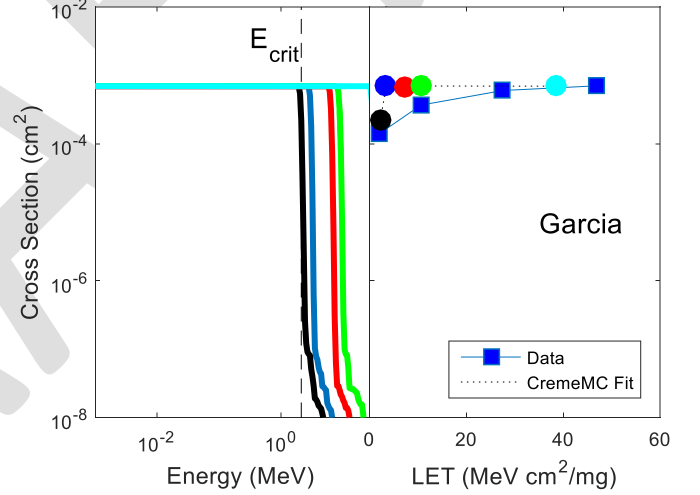

Fig. 10 Cross section curves generated by CREME-MC (left) and CREME-MC model compared to published data for [12]. Vertical dashed line indicates E_{crit} used to obtain the fit to the heavy ion data.

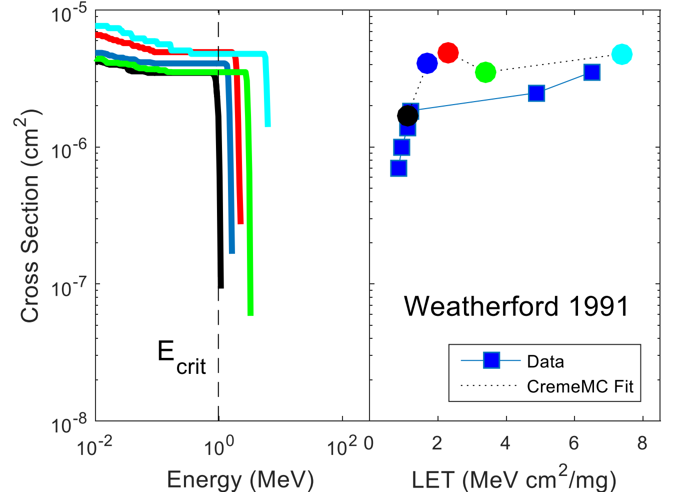

Fig. 11 Cross section curves generated by CREME-MC (left) and CREME-MC model compared to published data for [10]. Vertical dashed line indicates

DRAFT

E_{crit} used to obtain the fit to the heavy ion data.

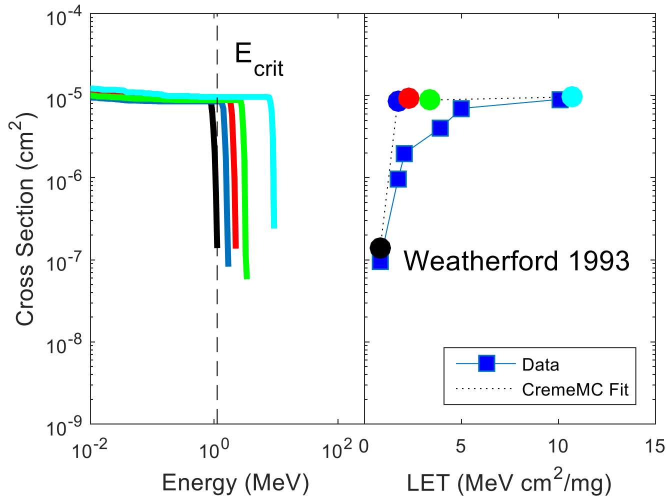

Fig. 12 Cross section curves generated by CREME-MC (left) and CREME-MC model compared to published data for [11]. Vertical dashed line indicates E_{crit} used to obtain the fit to the heavy ion data.

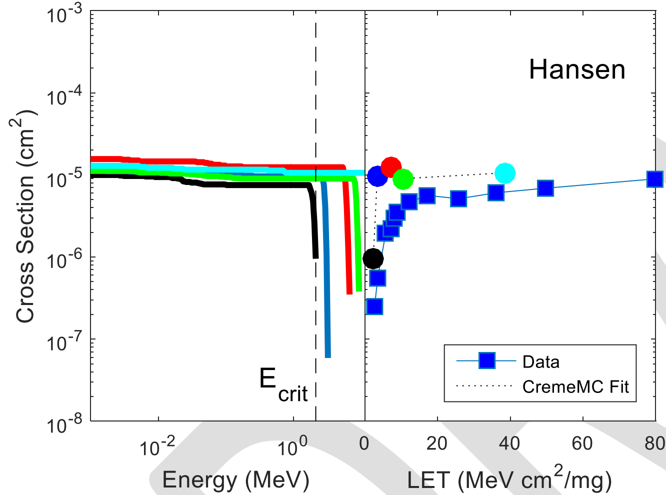

Fig. 13 Cross section curves generated by CREME-MC (left) and CREME-MC model compared to published data for [13]. Vertical dashed line indicates E_{crit} used to obtain the fit to the heavy ion data.

CREME-MC provides a good fit to the threshold and saturated cross-section of the heavy-ion cross-section data for the GaAs devices (Fig. 8 - 13). In most cases CREME-MC overestimates the cross section around the "knee" of the Weibull curve. For the cross-section vs. energy curves generated by CREME-MC (left side Fig. 8 – 13), the cross-section drops sharply above the curve knee. As a result E_{crit} calculated using Eq. 5 will be strongly affected by the LET of the ions simulated.

Simulating the irradiation of the device with protons and using the critical-energy values determined from the heavy-ion simulations provides the proton cross-section calculated using CREME-MC. The simulated proton cross-sections were calculated in "simplified" mode, with the heuristic multiplier for hadronic cross-section biasing (HCB) either set automatically or set manually between 100 and 10,000. This was necessary to ensure that the proton cross section curves extended to energies in the range of the E_{crit} calculated from the heavy ion curves. In general, the curves generated with the higher HCB multiplier give lower cross section values at the lower values for E_{crit}. At higher values of E_{crit}, especially in the range of E_{crit} values calculated for the device, the cross section curves generated with all values of HCB tend to converge. The results are shown in Fig 14 - 19. In these plots the values for E_{crit} calculated using Eq. 4 and derived from the CREME-MC simulations.

The results from the CREME-MC simulations are summarized in Fig. 20. In general, all calculated cross sections are within an order of magnitude of the measured cross-section. In most cases the CREME-MC simulations typically overestimate the measured cross section -- a useful feature in determining worst-case upset rates; however, they are not more accurate than the results from the other models (Table II). This is consistent with the fact that the data for the GaAs technologies was, for the most part, collected in a time frame commensurate with the development of the closed form models. As such the approximations made in developing these models were likely more applicable to these older technologies than they would be for newer, smaller devices.

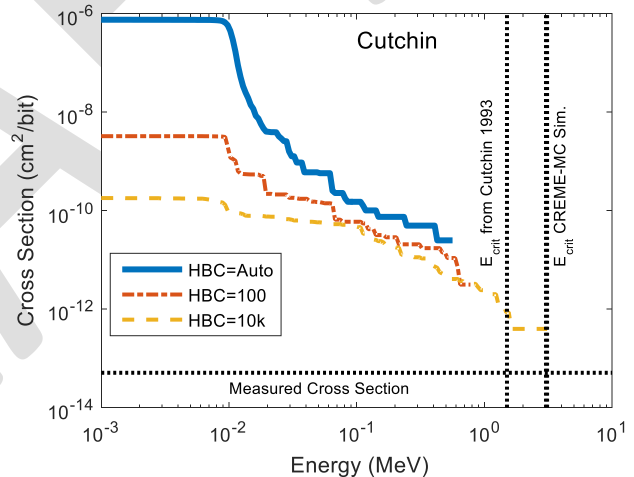

Fig. 14 Cross section as a function of E_{crit} for [8]. Vertical dashed lines indicate E_{crit} calculated by different methods. CREME-MC calculations are shown for different values of HCB.

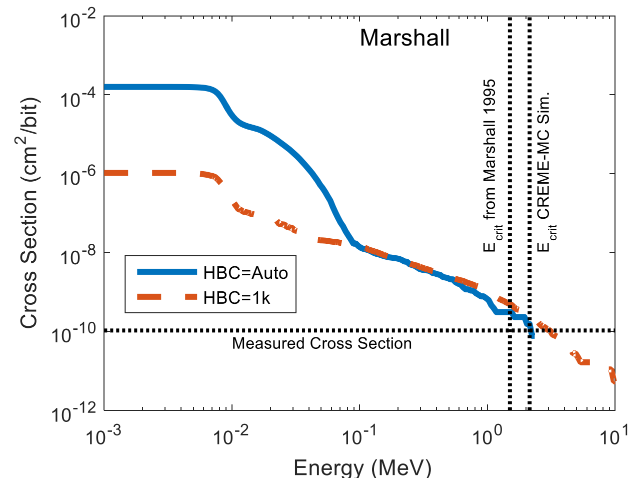

Fig. 15 Cross section as a function of E_{crit} for [9]. Vertical dashed lines indicate E_{crit} calculated by different methods. CREME-MC calculations are

DRAFT

shown for different values of HCB.

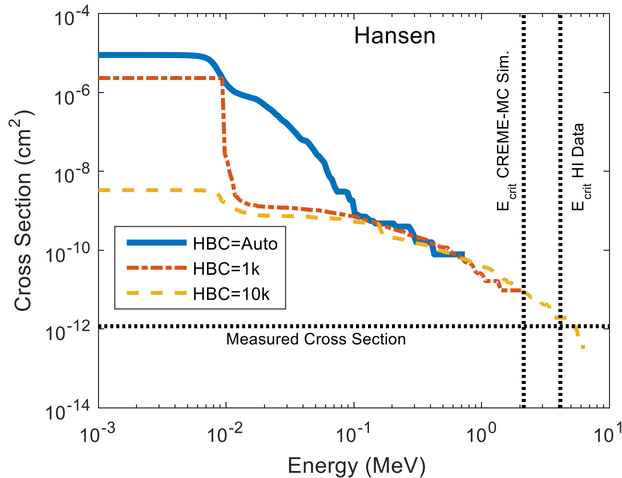

Fig. 16 Cross section as a function of E_{crit} for [13]. Vertical dashed lines indicate E_{crit} calculated by different methods. CREME-MC calculations are shown for different values of HCB.

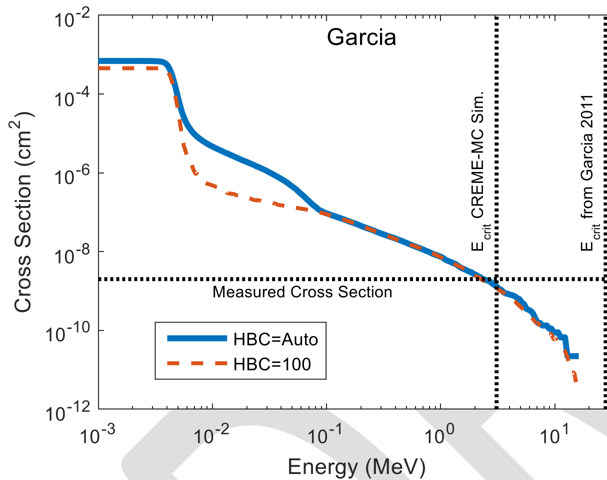

Fig. 17 Cross section as a function of E_{crit} for [12]. Vertical dashed lines indicate E_{crit} calculated by different methods. CREME-MC calculations are shown for different values of HCB.

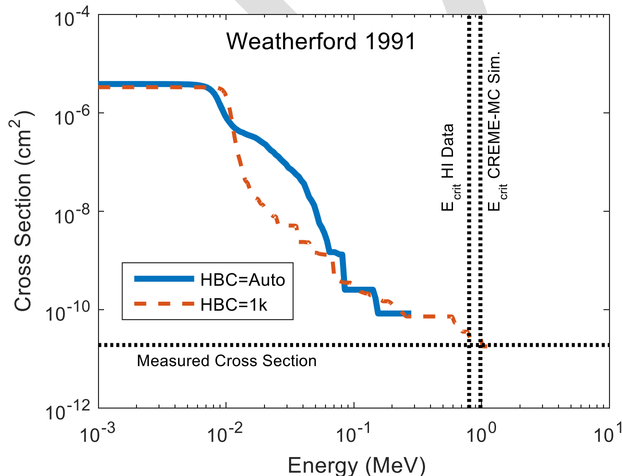

Fig. 18 Cross section as a function of E_{crit} for [10]. Vertical dashed lines indicate E_{crit} calculated by different methods.

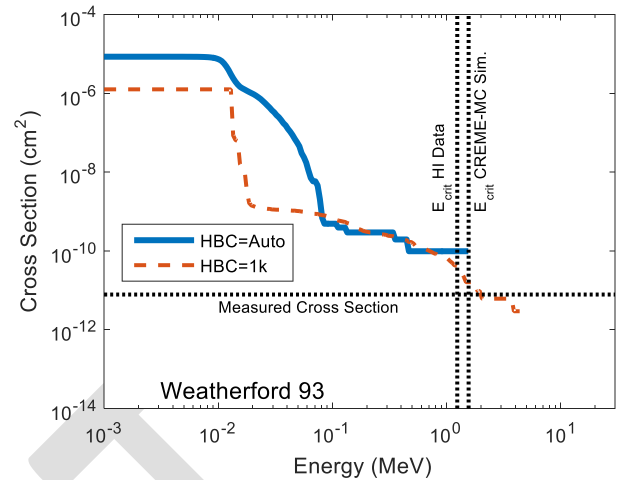

Fig. 19 Cross section as a function of E_{crit} for [11]. Vertical dashed lines indicate E_{crit} calculated by different methods. CREME-MC calculations are shown for different values of HCB.

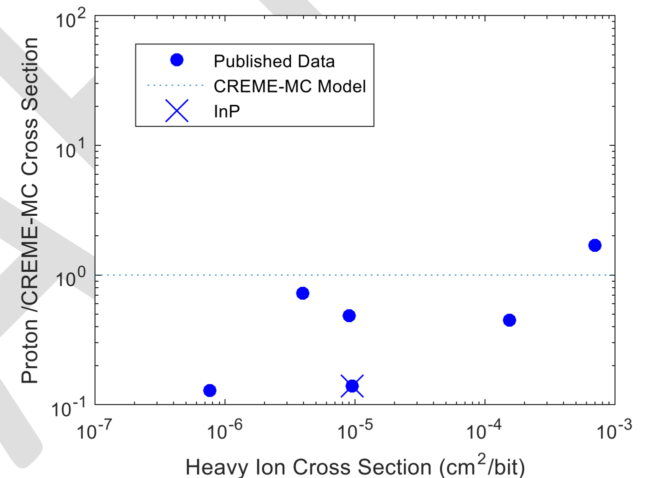

Fig. 20 Ratio of the proton data to the predicted proton cross section for the CREME-MC model

IV. Conclusion

Using data from the literature on a number of GaAs devices, we compared the effectiveness of a number of different models in predicting proton cross-section based on heavy-ion data. The closed form models and the CREME-MC models used were reasonably accurate, and able to estimate of the proton cross section within an order of magnitude. However, the additional computing time required to determine the CREME-MC results did not produce more accurate cross sections.

References

[1] P. Calvel, C. Barillot, P. Lamothe, R. Ecoffet, S. Duzellier, D. Falguere, "An empirical model for predicting proton induced upset," *IEEE Trans. Nucl. Sci.*, vol. 43, pp. 2827-2832, Dec 1996.

[2] L.D. Edmonds, "Proton SEU cross sections derived from heavy-ion test data," *IEEE Trans. Nucl. Sci.*, vol. 47, pp. 1713-1728, Oct 2000

[3] J. Barak, "Simple Calculations of Proton SEU Cross Sections from Heavy Ion Cross Sections," *IEEE Trans. Nucl. Sci.*, vol. 53, pp. 3336-3342, Dec. 2006.

[4] C. Weulersse, G. Hubert, G. Forget, N. Buard, T. Carriere, P. Heins, J.M. Palau, F. Saigne, R. Gaillard, "DASIE analytical version: A

predictive tool for neutrons, protons and heavy ions induced SEU Cross section," *IEEE Trans. Nucl. Sci.*, vol. 53, pp. 1876-1882, Aug. 2006.

[5] C. Inguimbert, S. Duzellier, T. Nuns, F. Bezerra, "Using subthreshold heavy ion upset cross section to calculate proton sensitivity," *IEEE Trans. Nucl. Sci.*, vol. 54, pp. 2394-2399, Dec. 2007.

[6] C. Weulersse, F. Wrobel, F. Miller, T. Carriere, R. Gaillard, J-R Vaille, N. Buard, "A Monte-Carlo engineer tool for the prediction of SEU proton cross section from heavy ion data," in *2011 Proc. 12th Eur. Conf. Radiat. its Effects Compon. Syst*., pp. 376-383.

[7] K.M. Warren, R.A. Weller, M.H. Mendenhall, R.A. Reed, D.R. Ball, C.L. Howe, B.D. Olson, M.L. Alles, L.W. Massengill, R.D. Schrimpf, N.F. Haddad, S.E. Doyle, D. McMorrow, J.S. Melinger, W.T. Lotshaw, "The contribution of nuclear reactions to heavy ion single event upset cross-section measurements in a high-density SEU hardened SRAM," *IEEE Trans. Nucl. Sci.*, vol. 52, pp. 2125-2131, Dec. 2005.

[8] J.H. Cutchin, P.W. Marshall, T.R. Weatherford, J. Langworthy, E.L. Petersen, A.B. Campbell, S. Hanka, A. Peczalski, "Heavy ion and proton analysis of a GaAs C-HIGFET SRAM," *IEEE Trans. Nucl. Sci.*, vol.40, pp.1660-1665, Dec 1993.

[9] P.W. Marshall, C.J. Dale, T.R. Weatherford, M. La Macchia, K.A. LaBel, "Particle-induced mitigation of SEU sensitivity in high data rate GaAs HIGFET technologies, "*IEEE Trans. Nucl. Sci.*, vol.42, pp.1844,1849, Dec 1995.

[10] T.R. Weatherfold, L. Tran, L.W.J. Stapor, E.L. Petersen, J.B. Langworthy, D. McMorrow, W.G. Abdel-Kader, P.J. McNulty, "Proton and heavy ion upsets in GaAs MESFET devices," *IEEE Trans. Nucl. Sci.*, vol.38, no.6, pp.1460,1466, Dec 1991.

[11] T.R. Weatherford, P.T. McDonald, A.B. Campbell, J.B. Langworthy, "SEU rate prediction and measurement of GaAs SRAMs onboard the CRRES satellite," *IEEE Trans. Nucl. Sci.*, vol.40, pp.1463-1470, Dec 1993.

[12] R. Garcia, E.J. Daly, H. Evans, P. Nieminen, G. Santin, B.D> Sierawski, M.H. Mendenhall, "Combined use of heavy ion and proton test data in the determination of a GaAs Power MESFET critical charge and sensitive depth," in *2011 Proc. 12th Eur. Conf. Radiat. its Effects Compon. Syst*. pp.244-251.

[13] D.L. Hansen, P.W. Marshall, R. Lopez-Aguado, K. Jobe, M.A. Carts, C.J. Marshall, P. Chu, S.F. Meyer, "A Study of the SEU Performance of InP and SiGe Shift Registers," *IEEE Trans. Nucl. Sci.*,, vol.52, pp.1140-1147, Aug. 2005.

[14] D.L. Hansen, P. Chu, S.F. Meyer, "Effects of data rate and transistor size on single event upset cross-sections for InP-based circuits," *IEEE Trans. Nucl. Sci.*, vol.52, pp.3166-3171, Dec. 2005.

[15] P. Chu, D.L. Hansen, B.L.Doyle, K. Jobe, R. Lopez-Aguado, M. Shoga, D.S. Walsh, "Ion-microbeam probe of high-speed shift registers for SEU Analysis-part II: InP," *IEEE Trans. Nucl. Sci.*,vol.53, pp.1583-1592, June 2006.

[16] M. Sokolich, M.Y. Chen, D.H. Chow, Y. Royter, S. Thomas III, C.H. Fields, D.A. Hitko, B. Shi, M. Montes, S.S. Bui, Y.K. Boegeman, A. Arthur, J. Duvall, R. Martinez, T. Hussain, R.D. Rajavel, J.C. Li, K. Elliott, J.D. Thompson, "InP HBT Integrated Circuit Technology with Selectively Implanted Subcollector and Regrown Device Layers," *IEEE Journal of Solid-State Circuits*, vol. 39, pp. 1615-1621, Oct. 2004.

[17] C.H.Tsao, R. Silberberg, J.R. Letaw, John, "A comparison of neutron-induced SEU rates in Si and GaAs devices," *IEEE Trans. Nucl. Sci.*, vol.35, pp.1634-1637, Dec 1988.

[18] J. Ziegler, J. Biersack, and U. Littmark, *The Stopping and Range of Ions in Solids*. New York: Pergaman, 1996.

[19] E. Normand, "Extensions of the burst generation rate method for wider application to proton/neutron-induced single event effects," *IEEE Trans. Nucl. Sci.*, vol.45, pp.2904-2914, Dec 1998.

[20] E. L. Petersen, "The SEU figure of merit and proton upset rate calculations," *IEEE Trans. Nucl. Sci.*, vol. 45, pp. 2550–2562, Dec. 1998.

[21] D.L. Hansen, "Proton Cross-Sections from Heavy-Ion Data in Deep-Submicron Technologies," *IEEE Trans. Nucl. Sci.*, vol.62, pp.2874-2880, Dec. 2015.

[22] on the web at https://creme.isde.vanderbilt.edu

[23] B.D. Sierawski, J.A. Pellish, R.A. Reed, R.D. Schrimpf, K.M. Warren, R.A. Weller, M.H. Mendenhall, J.D. Black, A.D. Tipton, M.A. Xapsos, R.C. Baumann, X. Deng, M.J. Campola, M.R. Friendlich, H.S. Kim, A.M. Phan, C.M. Seidleck, "Impact of low-energy proton induced upsets on test methods and rate predictions," *IEEE Trans. Nucl. Sci.*, vol. 56, pp. 3085-3092, Dec. 2009.

[24] R. Garcia, E.J. Daly, H. Evans, P. Nieminen, G. Santin, B.D. Sierawski, M.H. Mendenhall, "Calibration of the weighed sensitive volume model to heavy ion experimental data," *Proc. RADECS*, pp. 60-66, 19-23 Sept. 2011.

[25] R. Weller, M. H. Mendenhall, R. A. Reed, R. D. Schrimpf, K. M.Warren, B. D. Sierawski, and L. W. Massengill, "Monte Carlo simulation of single event effects," *IEEE Trans. Nucl. Sci.,* vol. 57, pp. 1726–1746, 2010.

[26] K. M. Warren, R. A. Weller, B. D. Sierawski, R. A. Reed, M. H.Mendenhall, R. D. Schrimpf, L. W. Massengill, M. E. Porter, J. D. Wilkinson, K. A. Label, J. H. Adams, "Application of RADSAFE to model the single event upset response of a 0.25µm CMOS SRAM," *IEEE Trans. Nucl. Sci*., vol. 54, pp. 898-903, 2007.

[27] C. Inguimbert, S. Duzellier, T. Nuns, F. Bezerra, "Using subthreshold heavy ion upset cross section to calculate proton sensitivity," *IEEE Trans. Nucl. Sci.*, vol. 54, pp. 2394-2399, Dec. 2007.

DRAFT